Simulation on Soot Deposition and Combustion in Diesel Particulate Filter

by

K. Yamamoto, S. Oohori, H. Yamashita

Department of Mechanical Science and Engineering, Nagoya University

Furo-cho, Chikusa-ku, Nagoya, Aichi 464-8603, JAPAN

S. Daido

Nippon Soken, Inc.

14 Iwaya, Shimohasum-cho, Nisho, Aichi 445-0012, JAPAN

(Abstract)

We have simulated the flow in a real cordierite DPF using the lattice Boltzmann method. Inner structure of the filter is analyzed by a 3D X-ray CT technique. Two processes of soot deposition for PM trap and soot combustion for filter regeneration process are considered. Especially, the effect of NO_2 on the soot oxidation is examined, which is recently proposed as on-board regeneration system. The reaction rate has been determined based on previous experimental data. The estimated values of Arrhenius factor and activation energy are A = 146 1/s, E = 79.5 kJ/mol with NO_2, and A = 1.20 1/s, E = 64.9 kJ/mol without NO_2. Results show that, the flow field and pressure change inside the filter are clearly visualized. The pressure distribution depends on the non-uniformity of pore structure. The flow is largely changed with soot deposition, with higher pressure drop across the filter (filter back-pressure). The obtained correlation between total accumulated soot and the filter back-pressure is well in accordance with reported experimental results. In combustion simulation, the effect of NO_2 addition to promote the soot oxidation is confirmed. These are useful information to develop the future regenerating DPF system.

Introduction

Nitrogen oxides (NO_x) and particulate matters (PM) including soot in diesel exhaust gas are severe environmental problems. It is expected that emission of soot particles can penetrate into the lung, causing human carcinogenic effects. To reduce these emissions especially from heavy-duty vehicles such as cargo trucks and buses, more strict exhaust emission standards such as Euro V in 2008 are being set in many countries. Recently, for the after-treatment of soot particles in exhaust gas, a diesel particulate filter (DPF) has been developed. One of the common types of DPF is a monolithic wall-flow filter. One example in **Fig. 1** is a cordierite filter used in this study. In simple explanation of DPF, it traps PM when exhaust gas passes its porous wall (**Fig. 1(b)**). It is the most efficient after-treatment device. Latest researches have shown that DPF filtration efficiency can be as high as 99 % [1-3]. However, the filter would be plugged with particles to cause an increase of filter back-pressure, which must be kept at lower levels, because the higher back-pressure increases fuel consumption and reduces available torque [4]. There are two methods, on-board and off-board regenerations. As for the off-board regeneration, the DPF is periodically replaced, or removed to eliminate hydrocarbons and particles by an electric heater. The system equipped with a temperature controller, compressed air source, and combustion devices is relatively large and complicated.

It is more appropriate to use the on-board regeneration, although it is still under development. It is passive regeneration, and its process is spontaneously conducted during the normal engine operation, which is called continuously regenerating trap (CRT). The filter surface is coated with noble metal catalysts such as platinum, mainly to reduce the temperature of soot oxidation [5]. So far, there are two approaches for on-board regeneration. One is to use a Ce-based fuel additive [6]. Its disadvantage is that, if the temperature is not sufficient, the presence of additive could prevent the direct soot oxidation by oxygen. Also, it should be substantially confirmed that the combustion products from Ce are not harmful to the environment.

We are focusing NO_x-soot conversion system, where PM is oxidized by catalyst indirectly. The

commercial DPF system such as Johnson Matthey CRT has been developed [7,8]. There are two stages for PM oxidation. At the first step, catalytic reactions oxidize NO in exhaust gas into NO_2. At the next step, NO_2 reacts with soot to produce CO and CO_2. Although soot is oxidized by NO and O_2, it has been pointed out that NO_2 is much more reactive for soot oxidation [9-11]. So far, the reaction rate and quantitative effect of NO_2 on soot oxidation have not been clear. To confirm the applicability of the above system, we need to understand the phenomena in the real wall-flow filter. Typically, the inlet size of filter monolith is about 2 mm, and the thickness of the filter wall where soot particles are removed is only 0.2mm. It is difficult to observe the small-scale phenomena inside the filter experimentally, and there is not enough information on the PM accumulation and reaction.

In this study, we simulate the flow in a real DPF by Lattice Boltzmann method (LBM). The structure of the cordierite filter is scanned by a 3D X-ray CT technique. The calculation domain is roughly shown in **Fig. 1**. By conducting tomography-assisted simulation, it is possible to discuss local velocity and pressure distributions in the real filter, which is hardly obtained by measurements. Two processes are included in the simulation. One is the soot deposition for PM trap. The other is the soot combustion to examine the filter regeneration with the catalytic effect. The reaction rate is evaluated from the previous experiments of soot oxidation with and without NO_2 [11].

Numerical method

3D X-ray tomography

Before simulating the flow in the real diesel filter, we obtained the inner structure by a 3D X-ray CT (Computed Tomography) technique. Non-destructive nature of the CT technique allows visualization of filter inner structure actually used. In our previous study [12,13], we have confirmed the applicability of the

tomography-assisted simulation. In the present simulation, we employed a similar data processing technique. **Figure 2** shows a CT image of the filter. The spatial resolution is 1 μm/pixel, which is the finest level in the reported CT measurements. Upper figure shows the image area of the filter in *x*-*y* plane, and lower figure shows digitized data used in simulation. Its total size is 400 μm (*x*) × 400 μm (*y*) × 200 μm (*z*). Complex porous structure with variety of pore size is well observed. Based on 3D CT data, it is found that the averaged porosity is about 0.4.

Lattice Boltzmann method (LBM)

We explain a numerical scheme for simulating fluid. So far, the LBM has been widely used, and has been an alternative and promising numerical scheme in fluid simulation [14]. It has been confirmed that, through the Chapman-Enskog procedure, the Navier-Stokes equations are derived from LB equations. In the LBM, the treatment of boundary conditions is simple and easy, and it is appropriate to simulate porous media flow [15-18]. In our previous study, we have conducted LB simulation of soot combustion for modeling filter regeneration process [19]. Here, the numerical scheme for the soot deposition is explained.

For flow field, an incompressible lattice BGK model of D3Q15 [20] is used. It should be noted that for combustion simulation, low Mach number approximation is adopted to consider the density change in the incompressible model. The detailed description is found in other papers [19,21-23]. The soot concentration in exhaust gas is determined by convection and diffusion. That is, the soot is transported by the mass flow rate due to the convective motion of gaseous mixture and the mass diffusion rate caused by the concentration gradient. In LB model, the above two transports are included [12,13].

$$F_{C,\alpha}(\boldsymbol{x}+\boldsymbol{e}_\alpha\delta_t,\ t+\delta_t)-F_{C,\alpha}(\boldsymbol{x},\ t)=-\frac{1}{\tau_C}[F_{C,\alpha}(\boldsymbol{x},\ t)-F^{eq}_{C,\alpha}(\boldsymbol{x},\ t)] \qquad (1)$$

$$F_{C,\alpha}^{eq} = w_\alpha Y_C \left\{ 1 + 3\frac{\boldsymbol{e}_\alpha \cdot \boldsymbol{v}}{c^2} + \frac{9}{2}\frac{(\boldsymbol{e}_\alpha \cdot \boldsymbol{v})^2}{c^4} - \frac{3}{2}\frac{\boldsymbol{v} \cdot \boldsymbol{v}}{c^2} \right\} \qquad (2)$$

where w_α = 1/9 (α = 1:6), w_α = 1/72 (α = 7:14), and w_{15} = 2/9, and $\boldsymbol{v}$=(v_x, v_y, v_z) is the local velocity vector. Eq. 1 is a transport equation for soot mass fraction, where F_C is the distribution function for soot mass fraction, and τ_C is the relaxation time determined by diffusion coefficient. In Eq. 2, $Fc,_\alpha^{eq}$ is the equilibrium distribution function. The soot mass fraction is obtained by the sum of the distribution function as $Y_C = \Sigma_\alpha F_{C,\alpha}$.

The approach for soot deposition is based on the modified particle deposition model [24]. In the simulation, it is impractical to consider the complex geometry and nano-size of soot particles. Different from Lagrangian approach by the equation of motion [25], individual particles are not considered. Instead, the soot mass concentration is monitored at the filter surface or deposited soot layer. Then, the mass fraction of deposited soot is given by

$$Y_{C,surface}(\boldsymbol{x} + \boldsymbol{e}_\alpha \delta_t,\ t + \delta_t) = \sum_\alpha F_{C,\alpha}(\boldsymbol{x},\ t) + Y_{C,surface}(\boldsymbol{x},\ t) \qquad (3)$$

where $Y_{C,surface}$ is the mass fraction of soot on the filter surface or deposited soot layer at each time step. Expectedly, $Y_{C,surface}$ is increased when the soot in gas phase accumulates. As the soot deposition is continued, the soot concentration sometime becomes unity. When this limit is reached, the solid site is piled up. The deposited soot region is treated as non-slip wall, which implies a dynamically change of boundary condition for fluid.

Figure 3 shows the calculation domain. The size is 400 μm (x) × 80 μm (y) ×80 μm (z), and the total number of grids is 401× 81× 81. The grid size is of 1 μm, which is the spatial resolution of the X-ray CT measurement. The diesel filter is placed in the center part in this calculation domain. The inflow velocity, U_{in}, is 100 cm/s, and the soot mass fraction at the inlet, $Y_{C,in}$, is 0.01. As for the boundary condition, the inflow

boundary is adopted at the inlet [20]. At the sidewall, the slip boundary condition is adopted, considering the symmetry [17]. At the outlet, the pressure is constant (atmospheric pressure, P_{out}), and the gradient of species concentration and temperature is zero. On the surface of the filter or deposited soot layer, bounce-back rule for non-slip wall is adopted.

Results and Discussion

Reaction Rate for Soot Oxidation

The rate of soot oxidation was estimated by previous experiments [11]. Temperature-programmed reactions (TPR) were carried out to evaluate the catalytic performance for soot oxidation. Commercially available carbon black (CB; Nippon Tokai carbon 7350F; primary particle size = 28 nm; specific surface area = 80 m^2/g) was used as model soot. The mixture of Pt/SiO_2 (0.5 g) and CB powder (0.005 g) were placed in the reactor. For the regeneration process with NO_2, 1000 ppm NO_2 was added in the flow. Other gases included were 0-7% H_2O, 10% O_2 and N_2, corresponding to the composition of diesel exhaust gas. The concentration of CO, CO_2, NO, and temperature, T, were monitored.

Figure 4 shows the test results for CB oxidation in the flow with NO_2. When CB is reacted with NO_2 as well as O_2, the combustion products of CO and CO_2 are formed. From this figure, it is found that the oxidation is initiated at 720 K and peak temperature for maximum oxidation rate is achieved at the temperature of 850 K. On the other hand, in the experiments without NO_2, TPR profile was much different. In this case, the oxidation is initiated at 760 K and peak temperature for maximum oxidation rate is around 940 K. Then, the oxidation of CB is much promoted by adding NO_2.

Next, we estimated the reaction rate of soot oxidation. Since there is enough oxygen burning off (oxidizing) the CB, it is assumed that the reaction rate is expressed by the reaction rate constant, k_r, and the

mass of CB. Then, by plotting the mass of reacted CB in the form of natural logarithm of the Arrhenius equation, reaction constants of Arrhenius factor, A, and activation energy, E, can be determined. It has been confirmed that, when $T > 650$ K, the concentration of NO_2 is in equilibrium values between NO and NO_2 when the Pt is present [11]. When the concentration of NO_2 is largely changed, the oxidation rate of CB could be varied. Therefore, we estimated the reaction constants in the temperature range of 670 K to 770 K. The obtained values are $A = 146$ 1/s, $E = 79.5$ kJ/mol with NO_2, and $A = 1.20$ 1/s, $E = 64.9$ kJ/mol without NO_2.

Soot Deposition

First, we examined the flow before soot deposition. **Figure 5** shows the velocity field inside the filter, which is under steady state with small velocity perturbation. The velocity vector is shown, with filter substrate by gray region. Three different slice images are shown at (a) $x = 40$ μm, (b) $x = 190$ μm, and (c) $x = 340$ μm. It is found that the ceramic filter has many small pores. Then, the velocity and its direction is largely changed when the flow passes through the filter wall.

We examined the pressure field along the flow direction (in x-axis), which is shown in **Fig. 6**. This pressure is the averaged value in y-z plane. For comparison, we checked the porosity in the calculation domain. The filter wall is located in the range of 50 μm $< x <$ 350 μm, and the porosity outside this region is unity. It is well known that, in case of homogenous porous media, the pressure linearly decreases along the flow direction, and the pressure gradient is constant. However, as seen in this figure, since the porosity inside the filter wall is largely varied from 0.2 to 0.6, the pressure gradient is changed. In particular, at the filter inlet, the steep pressure gradient is observed, mainly due to the smaller porosity. Therefore, depending on the non-uniformity of pore-structure, both flow and pressure are largely changed inside the filter wall.

Next, we simulated the flow with soot deposition. After a converged steady flow was obtained without soot deposition, the soot concentration at the inlet was given to observe the soot deposition

phenomena. **Figure 7** shows the flow field and accumulated soot in *x-y* plane at $z = 32$ μm (left figure) and in *y-z* plane at $x = 49$ μm (right figure). These profiles are obtained at $t = 104$, 311, and 518 μs, respectively. As already noted, the mass fraction of soot at the inlet, $Y_{C,in}$, is 0.01. First, the soot particle starts to deposit on the inside wall of the large substrate pore in **Fig. 7(a)**. Then, more deposited soot forms the pore bridging in **Fig. 7(b)**. Finally, a thin "cake layer" is developed at the filter inlet in **Fig. 7(c)**. At the same time, the velocity field is gradually changed. Especially, the velocity is largely accelerated in the narrow path caused by the soot deposition.

Figure 8 shows the pressure profile after soot deposition at $t = 518$ μs in **Fig. 7(c)**. This is the averaged pressure in *y-z* plane. For comparison, the pressure before soot deposition is also shown. It is found that only the pressure around the filter inlet, where soot is mainly accumulated, is increased. The similar pressure change is observed when the deposited layer is developed in the gas-particle flow [25].

We examined the correlation between total accumulated soot and pressure drop across the filter (filter back-pressure). Usually, this filter back-pressure is an important parameter for estimation of DPF filling with soot particles. **Figure 9** shows the relationship between total accumulated soot and the filter back-pressure. The accumulated soot is the mass of soot per unit filter volume. During simulation, the accumulated soot and pressure drop are monitored at each time step. It is found that, when more soot is accumulated in the filter, the filter back-pressure is expectedly higher.

Wirojsakunchai et al., have reported the experimental data to explain DPF filling process with PM trap by the conceptual model [3]. When PM starts to deposit in clean DPF via diffusion, impaction, and interception, PM is initially collected on the inside walls of the large substrate pore (stage 1). During this stage, pressure drop is not largely changed. When more PM accumulates, the pressure increases very largely due to the pore bridging (stage 2). After that, a thin "cake layer" of PM begins to develop at the filter inlet. In this case, a linear and slower pressure rise is observed as the cake layer thickens (stage 3). However, this model

has never been validated, because it is impossible to observe the soot deposition phenomena inside the filter.

To confirm the above explanation, the close-up details of the soot region in the range of 0 μm < x < 100 μm is shown in **Fig. 9**. In the pressure curve vs. deposited soot mass, three typical soot deposition profiles corresponding to stages 1-3 are shown. In this figure, the main deposited soot area is shown by a box or circle. It should be noted that filtration steps proposed in the above conceptual model are well observed in our simulation.

Soot Combustion for Filter Regeneration Process

Finally, the soot combustion was simulated for the filter regeneration process. For the initial soot distribution, the profile in **Fig. 7(a)** was used, where the accumulated soot is 1.14 g/l. Since it took more time to simulate the combustion field, smaller calculation domain was used. The area is of 20 μm < y < 60 μm and 20 μm < z < 60 μm in **Fig. 3**. In this simulation, the reaction rate evaluated by experiments was adopted to examine the catalytic effect of NO_2. The oxygen concentration is 10% in the inflow gas, which is the same value in the experiment. The temperature of inflow gas is 300 K. To initiate the soot reaction, the temperature of both filter region and deposited soot layer is increased to 1200 K. The time, t, is counted after we set this temperature.

Figure 10 shows the distributions in x-y plane of (a) filter region and deposited soot layer, (b) mass flux in x-direction, (c) pressure, and (d) temperature at t = 4 ms. These are the results with the reaction rate under NO_2 coexistence. In **Fig. 10(a)**, the light blue region is the filter substrate, and red region is the deposited soot layer. The velocity vector is also shown. The flow is accelerated due to the temperature rise. Since the heat release occurs due to soot combustion, the maximum temperature is higher than the initial soot layer temperature by 90 K.

To evaluate the effect of NO_2 on the soot oxidation, the combustion simulation is conducted using the reaction rates with and without NO_2. **Figure 11(a)** shows the mean temperature, which is the averaged value

on the surface of soot layer. For comparison, the mass of remained soot in DPF is shown in **Fig. 11(b)**. Since the reaction is very slow without NO_2, the slight temperature change is observed in this period, and most of soot is not reacted. In contrast, under NO_2 coexistence, the large temperature increase is observed. Resultantly, more soot is oxidized. From this comparison, it is clear that the soot reaction is largely accelerated in the flow with NO_2, and the effectiveness of regeneration process by NO_2 is confirmed in the simulation of real wall-flow DPF system. More recently, we have simulated NO-NO_2 conversion by catalyst with detailed chemistry [26]. In future, the appropriate temperature range in exhaust gas will be discussed to control the catalytic soot combustion effectively.

Conclusions

We have simulated the flow in the real cordierite DPF to examine the soot accumulation for PM trap and soot combustion for filter regeneration process. Inner structure of the filter has been obtained by a 3D X-ray CT technique. Especially, the effect of NO_2 on the soot oxidation is evaluated, which is recently proposed as the on-board regeneration system. The following results are obtained.

(a) Based on the experiments of soot oxidation, the estimated values of Arrhenius factor and activation energy are $A = 146$ 1/s, $E = 79.5$ kJ/mol with NO_2, and $A = 1.20$ 1/s, $E = 64.9$ kJ/mol without NO_2.

(b) Inside the filter, complex flow pattern along with pressure change is observed. The pressure distribution depends on the non-uniformity of pore structure. The flow is largely changed with soot deposition, with higher filter back-pressure.

(c) During DPF filling with soot, there are three stages: (1) soot deposition on the inside walls of large substrate pore, (2) pore bridging deposition, (3) a cake layer deposition at the filter inlet. According to these deposition processes, the pressure slightly changes, then rises abruptly, and slowly increases in the

pressure curve vs. deposited soot mass, which is in accordance with the reported experimental data.

(d) In combustion simulation, the filter regeneration process is well observed. When NO_2 is added, the soot oxidation rate becomes expectedly larger to burn more soot in the filter. The effectiveness of regeneration process by NO_2 is confirmed in the simulation of real DPF system.

These are useful information to develop future NO_x-soot regenerating DPF system in the after-treatment of exhaust gas.

Acknowledgement

This work was partially supported by New Energy and Industrial Technology Development Organization in Japan (Industrial Technology Research Grant, 05A18020d).

References

[1] J. C. Clerc, Applied Catalysis B 10 (1996) 99-115.

[2] A. G. Konstandopoulos, et al., SAE Technical Paper 2000-01-1016, 2000.

[3] E. Wirojsakunchai, et al., SAE Technical Paper 2007-01-0320, 2007.

[4] A. M. Stamatelos, Energy Conversion and Management, Vol.38(1) (1997) 83-99.

[5] S. Wang, and B. Haynes, Catalysis Communications 4 (2003) 591-596.

[6] G. C. Koltsakis and A. M. Stamatelos, AIChE J., 42(6) (1996) 1662-1672.

[7] B. J. Cooper, H. J. Jung, and J. E. Toss, US Patent, 4902487(1990).

[8] P. Hawker, Diesel emission control technology, Platinum Metals Rev. 39 (1995) 2-8.

[9] H. J. Stein, Applied Catalysis B 10 (1996) 69-82.

[10] G. Neri, et al., Applied Catalysis B 11 (1997) 217-231.

[11] J. Oi-Uchisawa, et al., Applied Catalysis B 21(1999) 9-17.

[12] K. Yamamoto, et al., Math. Computers in Simulation, 72 (2006) 257-263.

[13] K. Yamamoto, et al., Int. J. Modern Physics C, 18(4) (2007) 528-535.

[14] S. Chen and G. D. Doolen, Annu. Rev. Fluid Mech. 30:329-364 (1998).

[15] G. McNamara and G. Zanetti, Phys. Rev. Lett., **61** (1988) 2332–2335.

[16] A. Cancelliere, C. Chang, E. Foti, D.H. Rothman and S. Succi, Phys. Fluids A, **2** (1990) 2085–2088.

[17] T. Inamuro, M. Yoshino, and F. Ogino, Int. J. Numer. Methods Fluids 29:737-748 (1999).

[18] J. Bernsdorf, G. Brenner, and F. Durst, Comput. Phys. Commun. 129:247-255 (2000).

[19] K. Yamamoto, N. Takada, and M. Misawa, Proc. Comb. Inst. **30** (2005) 1509-1515.

[20] Q. Zou and X. He, X., Phys. Fluids 9 (6) (1997) 1591-1598.

[21] K. Yamamoto, X. He, and G. D. Doolen, J. Statistical Physics, Vol. 7, Nos.1/2 (2002) 367-383.

[22] K. Yamamoto and F. Ochi, J. Energy Institute 79, No.4 (2006) 195-199.

[23] K. Yamamoto and N. Takada, Physica A 362 (2006) 111-117.

[24] B. Chopard, A. Masselot, and A. Dupuis, Computer Physics Communications **129** (2000) 167-176.

[25] O. Filippova, and D. Hänel, Computers & Fluids **26** (1997) 697-712.

[26] T. Aikawa, H. Yamashita, K. Yamamoto, and H. Yane, Proc. Sixth Asia-Pacific Conf. Comb. (2007) 686-689.

List of figure captions

Figure 1 (a) Photograph of DPF, and (b) PM trap inside porous filter wall. Calculation domain is shown by dotted line.

Figure 2 Inner structure of DPF is obtained by X-ray CT technique. Upper figure shows the image area of the filter in x-y plane, and lower figure shows digitized data used in simulation.

Figure 3 Calculation domain and coordinate.

Figure 4 Combustion products at temperature programmed reactions (TPR) in 1000 ppm NO_2 + 7% H_2O + 10% O_2 in N_2.

Figure 5 Flow field and filter region shown by gray region; (a) x = 40 μm, (b) x = 190 μm, and (c) x = 340 μm.

Figure 6 Distributions of pressure and porosity across filter wall.

Figure 7 Profiles of flow field and deposited soot in x-y plane at z = 32 μm (left figure) and in y-z plane at x = 49 μm (right figure); (a) t = 104 μs, (b) t = 311 μs, and (c) t = 518 μs.

Figure 8 Pressure distributions before and after soot deposition.

Figure 9 Accumulated soot and pressure drop in DPF, together with soot region at three different stages.

Figure 10 Combustion field in x-y plane of (a) filter region and deposited soot layer with velocity vector, (b) mass flux in x-direction, (c) pressure, and (d) temperature; t = 4 ms.

Figure 11 (a) Mean temperature and (b) mass of remained soot in DPF to observe effect of NO_2 on soot oxidation.

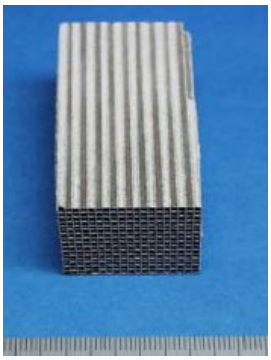

(a)

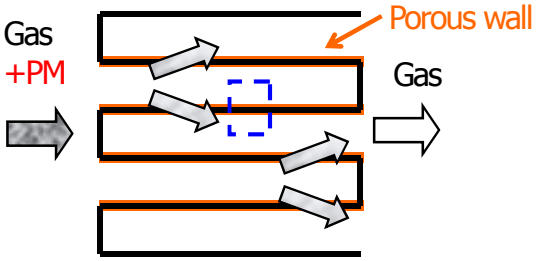

(b)

Fig. 1 (a) Photograph of cordierite DPF, and (b) PM trap inside porous filter wall. Calculation domain is shown by dotted line.

[Word Count] = (95+10)*2.2*1 + 22 (caption) = 253 words

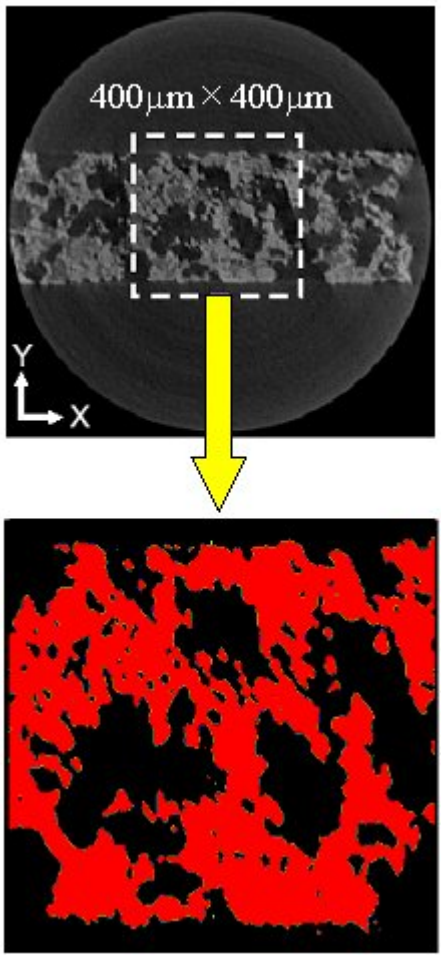

Fig. 2 Inner structure of DPF is obtained by X-ray CT technique. Upper figure shows the image area of the filter in *x-y* plane, and lower figure shows digitized data used in simulation.

[Word Count] = (125+10)*2.2*1 + 33 (caption) = 330 words

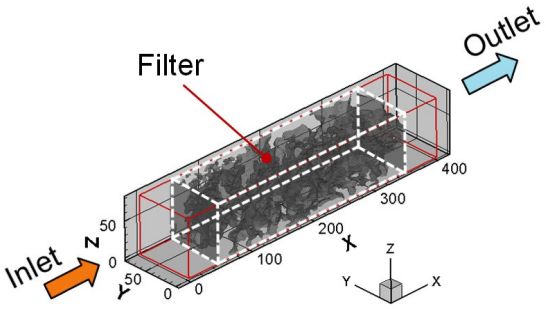

Fig. 3 Calculation domain and coordinate.

[Word Count] = (40+10)*2.2*1 + 6 (caption) = 116 words

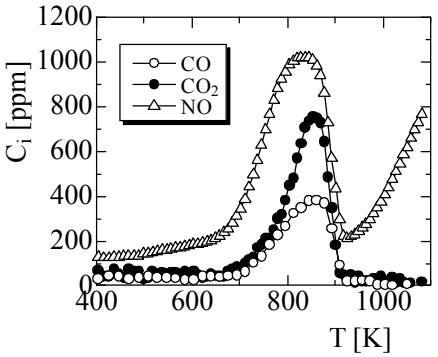

Fig. 4 Combustion products at temperature programmed reactions (TPR) in 1000 ppm NO_2 + 7% H_2O + 10% O_2 in N_2.

[Word Count] = (45+10)*2.2*1 + 21 (caption) = 142 words

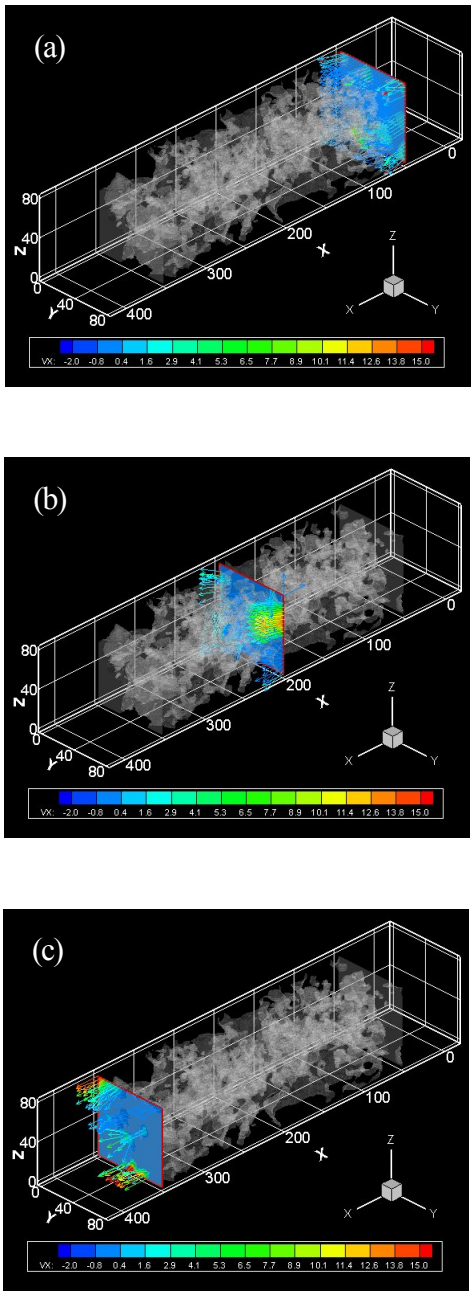

Fig. 5 Flow field and filter region shown by gray region;
(a) $x = 40$ μm, (b) $x = 190$ μm, and (c) $x = 340$ μm.

[Word Count] = (165+10)*2.2*1 + 25 (caption) = 410 words

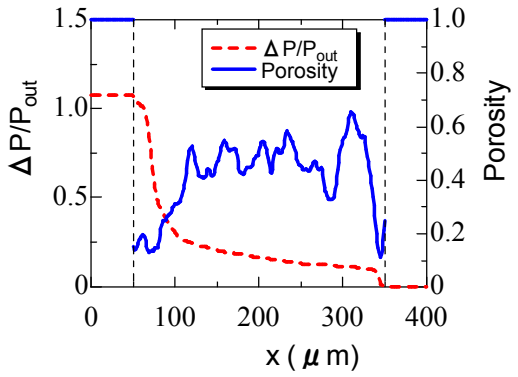

Fig. 6 Distributions of pressure and porosity across filter wall.

[Word Count] = (45+10)*2.2*1 + 10 (caption) = 131 words

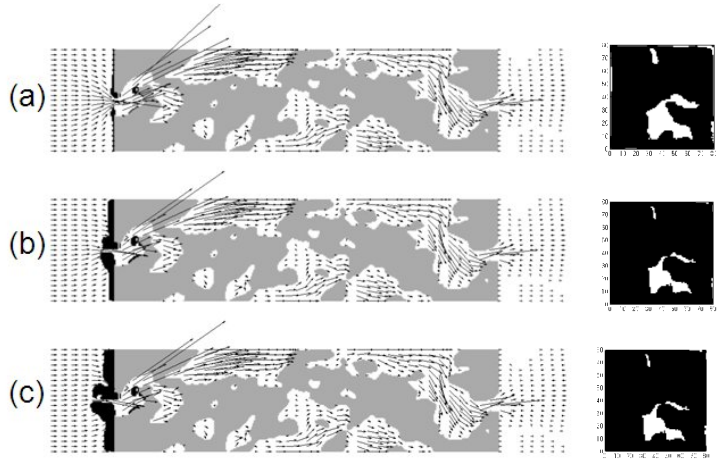

Fig. 7 Profiles of flow field and deposited soot in *x*-*y* plane at $z = 32$ μm (left figure) and in *y*-*z* plane at $x = 49$ μm (right figure); (a) $t = 104$ μs, (b) $t = 311$ μs, and (c) $t = 518$ μs.

[Word Count] = (55+10)*2.2*1 + 46 (caption) = 189 words

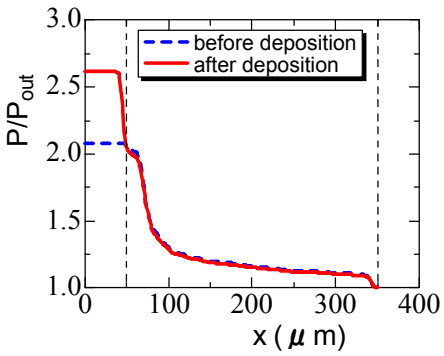

Fig. 8 Pressure distributions before and after soot deposition.

[Word Count] = (45+10)*2.2*1 + 9 (caption) = 130 words

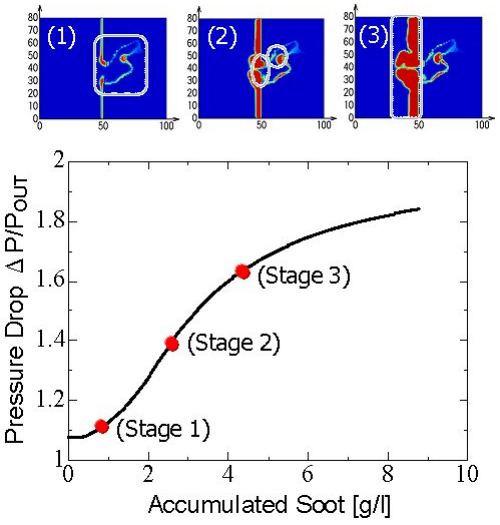

[Word Count]=(65+10)*2.2+17(caption) = 182 words

Fig. 9 Accumulated soot and pressure drop in DPF, together with soot region at three different stages.

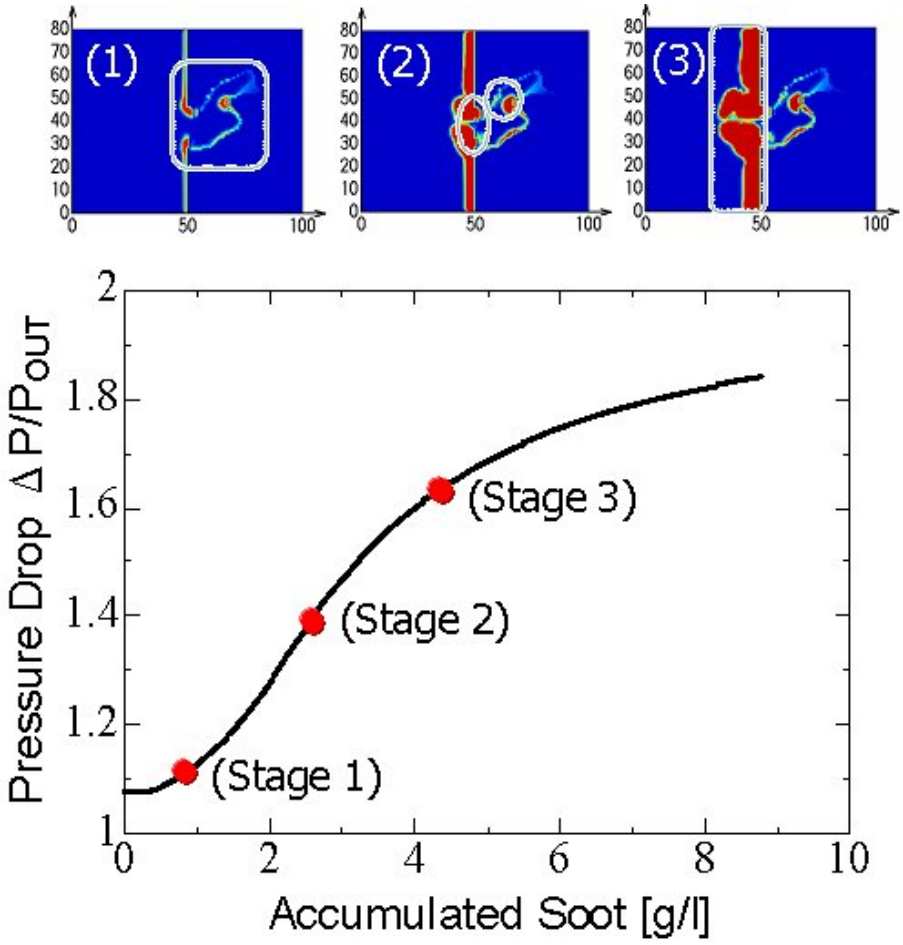

Fig. 9 (enlarged)

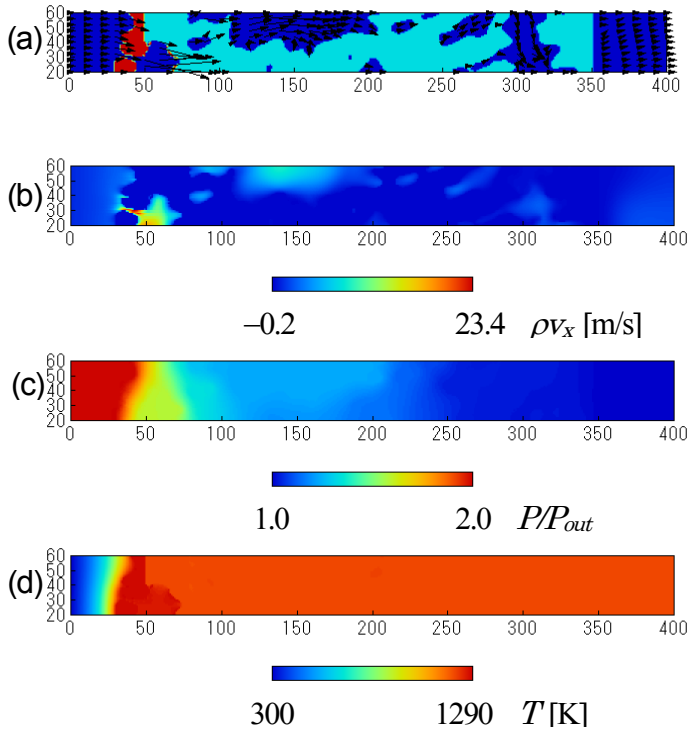

Fig. 10 Combustion field in *x*-*y* plane of (a) filter region and deposited soot layer with velocity vector, (b) mass flux in *x*-direction, (c) pressure, and (d) temperature; $t = 4$ ms.

[Word Count] = (95+10)*2.2*1 + 30 (caption) = 261 words

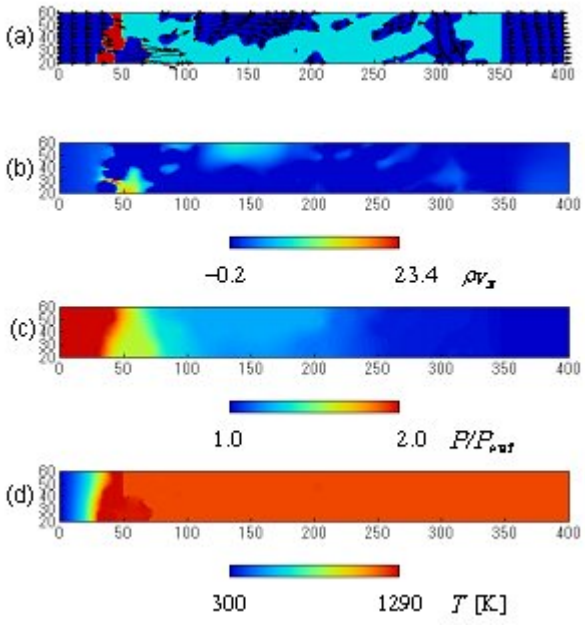

Lower figure is bmp version of Fig.10.

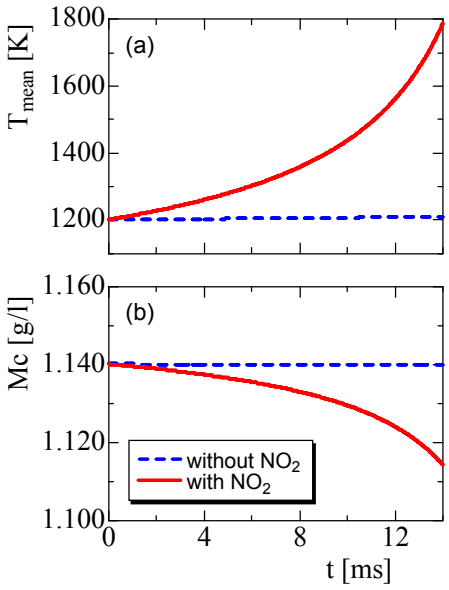

Fig. 11 (a) Mean temperature and (b) mass of remained soot in DPF to observe effect of NO_2 on soot oxidation.

[Word Count] = (75+10)*2.2*1 + 21 (caption) = 208 words